HHS Public Access

Author manuscript

Stem Cells. Author manuscript; available in PMC 2016 April 01.

Published in final edited form as:

Stem Cells. 2015 April ; 33(4): 1213–1229. doi:10.1002/stem.1937.

Cardiosphere Derived Cells from Pediatric End-Stage Heart Failure Patients Have Enhanced Functional Activity due to the Heat Shock Response Regulating the Secretome

Sudhish Sharma[1], **Rachana Mishra**[1], **David Simpson**[1], **Brody Wehman**[1], **Evan J. Colletti**[2], **Savitha Deshmukh**[1], **Srinivasa Raju Datla**[1], **Keerti Balachandran**[1], **Yin Guo**[1], **Ling Chen**[1], **Osama T. Siddiqui**[1], **Shalesh Kaushal**[3], and **Sunjay Kaushal**[1]

[1]Division of Cardiac Surgery, University of Maryland School of Medicine 110 S. Paca Street, 7th floor Baltimore, Maryland 21201, USA

[2]Department of Animal Biotechnology, University of Nevada, Reno, Nevada, 89557, USA

[3]Retina Specialty Institute, 6717 North 11[th]Place Suite C, Gainesville, Florida 32605 USA

Abstract

We have demonstrated that human neonatal cardiosphere derived cells (CDCs) derived from the young are more regenerative due to their robust secretome. However, it is unclear how the decompensated pediatric heart impacts the functional activity of their CDCs. Our aim was to characterize the potency of pediatric CDCs derived from normal functioning myocardium of control heart disease (CHD) patients to those generated from age matched end stage heart failure (ESHF) patients and determine the mechanisms involved. ESHF derived CDCs contained a higher number of c-kit$^+$, Islet-1$^+$, and Sca-1$^+$ cells. When transplanted into an infarcted rodent model, ESHF derived CDCs significantly demonstrated higher restoration of ventricular function, prevented adverse remodeling, and enhanced angiogenesis when compared to CHD patients. The superior functional recovery of the ESHF derived CDCs was mediated in part by increased SDF-1α and VEGF-A secretion resulting in augmented recruitment of endogenous stem cells and proliferation of cardiomyocytes. We determined the mechanism is due to the secretome directed by the heat shock response (HSR), which is supported by three lines of evidence. Firstly, gain of function studies demonstrated that increased HSR induced the lower functioning CHD derived CDCs to significantly restore myocardial function. Secondly, loss-of function studies targeting the HSR impaired the ability of the ESHF derived CDCs to functionally recover the injured myocardium. Finally, the native ESHF myocardium had an increased number of c-kit$^+$ CSCs. These findings suggest that the HSR enhances the functional activity of ESHF derived CDCs by increasing their secretome activity, notably SDF-1α and VEGF-A.

Correspondence should be addressed to: Sunjay Kaushal MD, Ph.D, Division of Cardiac Surgery, University of Maryland Medical Center, 110 S. Paca Street, 7[th] floor, Baltimore, MD 21201, skaushal@smail.umaryland.edu, Tel: 410-328-5842.

Disclosures

None

Introduction

Heart failure is a leading contributor of human morbidity and mortality in the developed world (1, 2). Additionally, heart failure within the pediatric population is also increasing in prevalence, contributing to higher mortality in children (3). This can likely be attributed to the heart being one of the least regenerative organs with a slow turnover of cardiomyocytes during the individual's lifespan. Thus, its ability to undergo repair after insult secondary to ischemia or other disease processes is significantly reduced (4). The identification and characterization of cardiospheres derived cells (CDCs) and c-kit^{+} cardiac stem cells (CSCs) have emerged as a promising cell based therapies for the functional recovery in diseased heart (5–9).

Currently, *ex vivo* expansion and transplantation of resident cardiac cells are the most widely studied methodologies to cause beneficial remodeling and restoration of the myocardial function. CDCs can be isolated and maintained by well-established protocols (10, 11), can be greatly expanded in culture, and show the ability to aid recovery of the injured myocardium when transplanted in a variety of animal models by differentiation into the three cardiovascular lineages: cardiomyocytes, vascular endothelial cells, and smooth muscle cells (5–7, 12, 13). CDCs consist of heterogeneous populations of cells containing partially differentiated and undifferentiated cells. These cells show distinct phenotypic profile (e.g. CD105^{+}>90%, CD45^{-}<1%). Phase I clinical studies using CDCs reported mild improvement in left ventricular ejection fraction but with marked reduction in scar formation and with improved regional systolic wall thickening (14).

Despite these encouraging results, many important biological questions remain regarding CDCs. Particularly, how does age and the de-compassionated state of the heart from which these cells are isolated effect the functional abilities of the CDCs. We have shown previously that neonatal derived CDCs outperform adult derived CDCs in their ability to functionally improve the ischemic rodent myocardium (15). It has been unclear how pediatric end stage heart failure (ESHF) derived CDCs will functionally perform when delivered to damaged myocardium in a comparative study to age-matched, control heart disease (CHD) derived CDCs which are from ventricular septal defect patients with normal functioning myocardium or from donor myocardium at the time of heart transplantation. Previous reports showed enhanced proliferation of cardiomyocytes derived from ESHF heart as compared to normal heart (16, 17). It has also been reported that the ESHF heart returns to a fetal gene expression program as an attempt for better survival (18). These studies suggest that the ESHF derived CDCs may have different qualitative functional abilities when compared to CHD derived CDCs. Recently, it was reported that adult derived CDCs from ESHF patients showed a stronger recovery of the injured myocardium, more than age match controls, which was attributed in part to increased beneficial cytokine secretion. However, the exact mechanism for the increased cytokine secretion was never determined (19, 20). Cumulatively, these reports suggest that all CDCs are not functionally equivalent and may be influenced by other factors, including age or the intrinsic physiologically state of the heart.

In the present study, we tested whether pediatric ESHF derived CDCs are more efficacious when compared to age-matched CHD derived CDCs in their ability to recover injured myocardium. We further determined via three lines of evidence that the HSR, up regulated in the ESHF derived CDCs, is a key regulator and determinant for this improved functional activity. We showed that in a gain of function study, the HSR stimulated the lower potent CHD derived CDCs to increase significantly their secretion of SDF-1α and VEGF-A, among other cytokines, and induce higher recovery of the ischemic injured myocardium. Next we demonstrated that when the heat shock response (HSR) is blocked by siRNA targeting HSF-1, the master regulator of the HSR, there is significantly decreased cytokine production, resulting in decreased functional myocardial recovery. Finally, we show that the native ESHF myocardium increased the number of endogenous c-kit$^+$ CSCs. These findings show that the ESHF derived CDCs have a higher functional activity compared to CHD derived CDCs, and that this phenomena is dependent on the HSR pathway. These data support the conclusion that the HSR is an integral pathway regulating the functional potency of CDCs, a finding not previously described to our knowledge.

Materials and Methods

Human tissue samples

The Institutional Review Committee at the University of Maryland and Lurie Children's Hospital, Chicago, approved this study. After parental consent was given, heart tissue was obtained from hearts of patients with different diagnosis (Table 1). Tissue specimens (n=14) were obtained from the right atrial appendage (RAA) of explanted end-stage heart failure (ESHF) hearts or aged-matched pediatric control heart disease (CHD) hearts either from donor hearts (DNR, N=7) at the time of heart transplant or from ventricular septal defect hearts (VSD, N=7) that have normal functioning myocardium and these patients are undergoing routine congenital heart surgery for a VSD repair.

Generation of CDCs

Human CDCs were generated using the protocol described previously (7) and with our modifications (12). Briefly, right atrial appendage (RAA) samples from ESHF or CHD myocardium were chopped into pieces ranging from 1.0 to 2.0 mm in diameter and treated with digestion buffer [collagenase type II (1mg/ml) (Worthington Biomedical Corp, Lakewood, NJ) and dispase (0.8mg/ml) (Gibco) suspension made in 0.05% trypsin/EDTA)]. Explants were plated on fibronectin-coated flasks in explant media [Iscove modified Dulbecco medium (IMDM) with 20% FBS, antibiotics and 100μM β-mercaptoethanol]. After 2 to 3 weeks, the desired phase-bright cells originating from explants were removed by mild trypsinzation and plated on poly-D lysine coated flasks at low density (1.5 to 3 $\times 10^4$ cells/mL) in cardiosphere-growing medium (CGM)(7). After a week of culture, the phase-bright cells formed cardiospheres, which were detached and expanded on fibronectin coated flasks in explant medium.

Generation of c-kit$^+$ cells

C-kit$^+$ cells were isolated from RAA samples of ESHF or CHD myocardium by using previously described protocol (21). Briefly, samples were minced in Ham's F12 medium

(Lonza #12-615F) and digested with 1–2mg/ml of Collagenase type II (Worthington # 4177) and incubated on a shaker for 30 – 45 min at 37°C. Following the collagenase treatment, cells were washed twice with growth medium [Ham's F12, Fetal Bovine Serum (10%), recombinant human FGF-basic (10 ng/ml), L-glutathione (0.2mM), human erythropoietin 250 (5U/ml)] before being plated. At sub confluencey, cells were trypsinized and sorted for c-kit$^+$ cells with Miltenyi microbeads (CD117 MicroBead Kit human #130-091,332) as per the kit instructions. The c-kit$^+$ cells were collected and cultured in growth medium as mentioned above.

Treatment of Cells

CDCs or c-kit$^+$ cells were treated with 300nM celastrol (CEL) (Gaia, Inc.) or 100nM triptolide (TTD) (Sigma-Aldrich) for 24 hrs before further testing. For heat shock (HS) treatment, cells were incubated for 4 hours at 42°C followed by 24 hours recovery incubation at 37°C before further testing.

RNA extraction and RT-PCR analysis

Total RNA was isolated from cells or tissues using RNeasy Kit (QIAGEN) according to the manufacturer's instructions. 500ng RNA/reaction was reverse-transcribed using cDNA synthesis kit according to the manufacturer's protocol (Applied Biosystem). 5 ng cDNA was used for each sample in a 20 μl PCR reaction. Each reaction was performed in triplicates using a ABI Fast SYBR-Green reaction mix on StepOnePlus® (Applied Biosystem, CA) PCR machine. Quantitect primer assays for each primer set were obtained from Qiagen. The C_T values of the housekeeping gene (ribosomal 18s) were subtracted from the corresponding gene of interest (ΔC_T). The fold change of expression level for each gene was determined by the expression $2^{-\Delta\Delta C_T}$. The final values were averaged and results were represented as fold expression with the standard error.

Flow cytometry analysis

CDCs and c-kit$^+$ cells at P3 were labeled with fluorochrome-conjugated primary antibodies (c-kit$^+$ and Ki67 (BD Pharmingen), Sca-1 (Cedarlane), FLK1 and CD105 (R&D systems) for one hour at room temperature. Appropriate isotype controls were prepared for each immunosubtypes. The labeled cells were evaluated for flow cytometry with Becton-Dickinson FACS caliber (San Jose, CA) with 25,000 events collected.

Cell transplantation, echocardiography and hemodynamic measurement

Myocardial infarction was induced by permanent ligation of the left anterior descending (LAD) coronary artery in immunodeficient male rats (weight, 250–300 g). The heart was exposed via a left thoracotomy, and the proximal LAD was ligated. Afterward, 1 million cells of either ESHF derived CDCs, ESHF-HSF-KD CDCs (ESHF derived CDCs with HSF1 Knockdown), CHD derived CDCs, HS or CEL treated CHD derived CDCs, or control cardiac fibroblasts, suspended in 250 to 400μL of vehicle (IMDM) were injected into the myocardium at four adjacent sites to the infract. One rat surgeon performed the MIs in figure 2A and 5L using the VisualSonics Vevo 770 ultrasound unit and another rat surgeon performed the MIs in figure 6L using the VisualSonics Vevo 2100 ultrasound unit

(VisualSonics, Toronto, Canada). Baseline echocardiograms were acquired at 1 day before myocardial infarct surgery. Echocardiographic examinations were also performed at 7 days and at 4 weeks post-myocardial infarction. Two-dimensional and M-mode echocardiography was used to assess fractional area change (FAC). Images were obtained from the parasternal long axis and the parasternal short axis at the midpapillary level. We observed some discrepancies in the echocardiographic findings using the same injected cells (Figure 2A and 5L versus Figure 6L), which was due to the two different rat surgeons using different echocardiography systems. However, each surgeon performed all rat surgeries in a blinded, randomly assigned order with no overlap between the two different studies. Hemodynamic measurements were done as previously described (23). Briefly, after the final echocardiographic examination, rats were anesthetized with 1% isoflurane, a median sternotomy was performed and pressure-volume conductance catheter (FT212, SciSense, Canada) was inserted through carotid artery into LV. Aortic and left ventricular pressures were recorded using Scisense ADV500 pressure-volume control. To assess for consistency in our MI model, a subset of rats were randomly assigned to euthanasia 1 day following MI (control: n=3, ESHF-derived CDCs: n=3, CHD-CDCs: n=3). These subgroups underwent echocardiography (Vevo2100).

Immunohistochemistry and Immunocytochemistry

Tissues were processed as described previously (12). Briefly, rat hearts were excised after hemodynamic data collection under anesthesia and perfused with 4% paraformaldehyde. Human tissue was fixed with 4% paraformaldehyde. Tissues were cryo-preserved using 30% sucrose and embedded in OCT (TissueTek). Sections were cut to 7μm, using a commercial cryostat, and stained for isolectin B4 (Invitrogen; Carlsbad, CA), α-SMA (Sigma), sarcomeric-α-actin (Santa Cruz Biotechnology; Santa Cruz, CA), anti-human nuclei (Millipore; Billerica, MA), or c-kit^{+} (BD Biosciences) primary antibodies. For Isl-1 staining, the cells were fixed with 4% PFA, permeabilized, overnight incubated with Isl-1 antibody (R & D Systems), incubated with FITC labeled secondary antibody. Cells and tissue sections were counterstained with DAPI (4’,6-diamidino-2-phenylindole) nuclear stain (Sigma; St Louis, MO).

Myocardial Viability

To calculate infarct size, Masson Trichrome–stained sections at various levels along the long axis were analyzed for collagen deposition. The midline technique for infarct size determination was used as described previously (15). With the use of ImageJ software, the viable myocardium was then calculated within the overall infracted zone by the number of red pixels (viable tissue) divided by overall number of pixels.

Paracrine Factor Quantification

CDCs at P3 were grown in complete explant media till they reached 85% confluence (~1×106 cells). The condition medium was concentrated using 3KDa filters (Millipore Inc) and protein content was quantified using BCA method (Pierce Inc). To normalize the protein content we used the following formula: (Concentration factor) × (total volume of medium)/ total protein content of conditioned medium (24). CDCs were treated with 300nM CEL for 24 hours or heat shock (42°C for 4 hours). Complete medium was replaced in treated or

untreated CDCs with FBS free basal medium (IMDM) and conditioned for next 72 hours. The conditioned medium was collected and concentrated using 3kDa filtration unit (Millipore Inc.). The conditioned medium was quantified using BCA method and normalized to total of 1mg protein. ELISA was performed for human VEGF-A, SDF-1α, PDGF-A, IL-6, ANG-2, FGF-2, LIF, IL-1, HGF-1, IGF-1, and SCF in the core facility at University of Maryland using human-specific ELISA kits (Millipore and R&D systems Inc.), according to the manufacturer's protocol.

Angiogenesis, apoptosis, and Cell Proliferation assay

The formation of tube-like structures was assessed in a Matrigel coated 96 well plate (BD Biosciences) as described previously (24). Briefly, HUVECs were plated on Matrigel for 4 hours before the addition of endothelial cell media (Lonza), as positive control, or with conditioned media from either ESHF derived CDCs, CHD derived CDCs, CEL or HS treated CHD derived CDCs, IMDM, Cfb or ESHF-HSF-KD CDCs. Cells were imaged after 12 hours to reconstruct the complete image of every well. The total tube length was then measured with the ImageJ plug-in, NeuronJ (NIH) (http://rsb.info.nih.gov/ij). The assessment of cell proliferation was performed by MTS assay (CellTiter 96 Aqueous One Solution Cell Proliferation Assay Kit, Promega) as per the manufacturer’s instruction (25). The assessment of apoptosis was performed per manufacture instructions for TUNEL (Milipore)

Immunoblot analysis

Cells were lysed with the RIPA buffer (20mM Tris-HCl (pH 7.5), 150mM NaCl, 2.5mM sodium pyrophosphate, 1mM Na_2EDTA, 1mM EGTA, 1% NP-40, 1% sodium deoxycholate, 1mM β-glycerophosphate, 1mM Na_3VO_4, 1μg/ml leupeptin, Cell Signaling Technology®) containing a complete protease inhibitor cocktail (Roche Applied Science). Cell lysate was prepared and protein concentration was determined using the BCA method (Thermo Scientific). 40μg of protein lysate was resolved on 4–12%SDS-PAGE, transferred to PVDF membrane using semidry or wet transfer method and probed with the indicated specific antibodies. The membrane were probed with antibodies to hsf1 (BD biosciences) HSP70, HSP27 (Enzo lifesciences), c-kit$^+$ (Novus), ISL-1 (Sigma-Aldrich), VEGF-A (Santacruz) and GAPDH (Millipore). We have analyzed 5 biological replicates for immunoblot analysis. The Odyssey system from Li-cor biosciences was used for detection and quantitative analysis.

siRNA Transfection

CDCs were seeded in 6 wells plate at approximately 50,000 cells and allowed to reach ~60% confluency before transfection. The siRNA duplexes for human-HSF1 (Cat # s6950) and scrambled non-targeting siRNA (Silencer select negative control cat # 4390844) were obtained from Ambion. Cells were mock transfected or transfected with corresponding 100 nM siRNA using Lipofectamine or Lipofectamine RNAiMax (Invitrogen Inc) according to the manufacturer's transfection protocol. Knockdown efficiency was evaluated after 48 hours for RNA and protein expression. Conditioned medium was collected after 96 hours of siRNA transfection for ELISA analysis.

Statistical Analysis

Data were analyzed using GraphPad Prism 5 software. When comparing two conditions, we used student's *t*-tests (non-parametric) with Mann-Whitney's test. More than two comparisons were made using one-way ANOVA (non-parametric) followed by Dunns post hoc or Tukey,s test. Two-way ANOVA with Bonferroni correction was used for grouped analysis of ECHOs data. Probability values of less than 0.05 were considered significant and tests were performed two-sided. Data are presented as mean and error bars depict the standard error of the mean (s.e.m.)

Results

Biochemical Confirmation in ESHF myocardium

All explanted human transplanted hearts were from pediatric patients in conditions of severe heart failure with New York Status Classification between III and IV and all with ventricle ejection fraction less than 20%. The etiologies of the pediatric ESHF patients varied in diagnosis from idiopathic or dilated cardiomyopathy to burnt-out congenital heart disease cardiomyopathy (Table 1) To confirm their biochemical properties, we determined the distinctive failing heart expression profile of key genes in the ESHF myocardium and in age-matched CHD myocardium (18, 26, 27).

When compared to age-matched CHD myocardium, which have normal functioning myocardium, ESHF myocardium had a reduction of α-MHC mRNA expression by 4.5 fold ($P<0.001$) and up regulated β-MHC by 7.5 fold ($p<0.05$). The expression of atrial natriuretic factor (ANF) was enhanced by 8 fold ($P= 0.0159$, supporting information Fig. S1A–B) in ESHF tissue, which is consistent with the switch to the fetal gene expression program. These results confirmed that all the study patients truly had ESHF both at a clinical and biochemical level and the CHD patients had no biochemical evidence of heart failure.

Characterization and Comparison of CDCs derived from CHD and ESHF Myocardium

We isolated CDCs from the right atrial appendage (RAA) of CHD and ESHF myocardial specimens using our previously modified protocol requiring explant plating, cardiosphere generation, and replating for CDC expansion (12). From these cardiospheres, CDCs could be expanded beyond 30 days and yielded greater than 2×10^6 cells. Even RAA myocardial samples weighing between 20 to 40 mg generated similar cell numbers using our current modified CDCs manufacturing protocol. The two different types of CDCs derived from CHD or ESHF myocardium had the same cellular morphology, isolation characteristics, and growth potentials as measured by doubling time (Fig. 1A, 1B). These results indicated that the generation and expansion of the CDCs was independent of patient diagnosis. Next, CDCs were examined for their expression of stemness markers and cardiac lineage commitment markers to determine whether the expanded CDCs remained in an uncommitted state or differentiated state. ESHF derived CDCs showed statistical significantly higher number of c-kit$^+$ cells (CHD n=5, 3.06 ±0.4% vs. ESHF, n=5, 9.36±1.38%, P=0.0079) and Sca-1$^+$ cells when compared to CHD derived CDCs (CHD n=6, 2.62 ±1.06% vs. ESHF, n=5, 7.78 ±1.74%, P=0.041, Fig. 1C, 1D). There were no discernable differences observed for CD105, Ki-67 and FLK1 expressing cells from the

various sources (Fig. 1E–G). CDCs were found to be negative for CD45 and CD31 (supporting information Fig. S2). Because the Islet-1 (Isl-1) antibody was not conducive for flow cytometric analysis, the number of Isl-1^+ cells was determined by quantitative immunofluorescence. ESHF derived CDCs significantly increased the number of ISL-1^+ cells when compared to CHD derived CDCs (CHD n=4, 3.71 ±0.093% vs ESHF, n=4, 16.36 ±2.4%, P=0.0025, Fig. 1H). We further showed that each of the CDCs derived from ESHF patients had higher number of c-kit^+ cells in comparison to CDCs derived from age-matched CHD patients by more than two-fold (****P<0.0001, Fig. 1I). These results indicated that the ESHF derived CDCs had a higher prevalence of c-kit^+, Sca-1^+, and Isl-1^+ CSCs in comparison to CHD derived CDCs.

ESHF derived CDCs display a strong functional potential

To determine whether the increased number of c-kit^+, Sca-1^+, and Isl-1^+ CSCs in the ESHF derived CDCs correlated with improved functional potential, we performed a randomized blinded study to evaluate the effectiveness of transplanted CDCs to improve acute infarcted myocardium in an immunodeficient rat model. Since the human CDCs were tracked for their expression of human nuclear antigen, this study also represented a lineage tracing experiment in the rodent myocardial infarct (MI) model to determine their final identity within the myocardium. After the left anterior descending artery ligation, CDCs, cardiac fibroblasts, or Iscove modified Dulbecco medium (IMDM; control) were injected. The consistency of our MI model was verified for each treatment group by performing random echocardiography at baseline and 24 hours after MI (supporting information Fig. S3). We observed no difference in EF between the 3 groups at baseline or 24 hours post-MI that signified all MIs performed were consistently among all three groups. Echocardiography performed at day 7 after LAD ligation revealed a higher preserved left ventricle ejection fraction in hearts transplanted with ESHF derived CDCs compared to controls, cardiac fibroblasts (Cfb), and CHD derived CDCs from VSD patients (ESHF, n=6: 52.03±6.9% vs CNT, n=6: 29.5±4.6%, P<0.0001; vs Cfb, n=4: 32.9±9.1%, P<0.01 and vs CHD, n=6: 40.9±4.3%, P<0.05, Fig. 2A). Differences between CHD derived CDCs, cardiac fibroblasts, or control treated hearts did not reach statistical significance. The improved left ventricle function was sustained from 7 to 28 days and signified the lasting effect of the transplanted ESHF derived CDCs (ESHF, n=6: 55.9±7.9% vs control, n=6: 30.3±3.8%, P<0.0001; vs Cfb, n=4: 28.7±3.1%, P<0.0001 and vs CHD, n=6: 42.98±4.2%, P<0.01) In a separate experiment, the functional recovery potential of ESHF derived CDCs was directly compared to CDCs derived from the respective donor heart at the time of transplantation (DNR), which represents another age-matched cohort with CHD myocardium. Even though there was no difference at 7 days, transplanted ESHF derived CDCs significantly preserved the ejection fraction when compared to transplanted DNR derived CDCs after 28 days (ESHF, n=3: 56.7±3.9% vs DNR, n=3: 41.9±4.7%, P<0.05, Fig. 2B). Furthermore, transplanted ESHF derived CDCs led to significantly improved hemodynamic contractility compared to control and transplanted CHD derived CDCs as determined by dP/dt, the rate of rise of left ventricular pressure (ESHF, n=6, −9191±354.9 vs CNT, n=4, −7677±346.4, P<0.05;ESHF, n=6, −9191±354.9 vs CHD, n=7, −8068±265.5, P<0.05, Fig. 2C). Transplanted ESHF derived CDCs also showed an improvement in +dP/dt, a measure of diastolic relaxation at 28 days as compared to control (CNT, n=4, 6529±440.5 vs ESHF, n=6,8670±529.7,P<0.05;

CNT, n=4, 6529±440.5 vs CHD, n=7, 8412±412.7, $P<0.05$, Fig. 2D). Additionally, we quantified scar formation by histological evaluation of myocardial sections with Masson's trichrome to determine the extent of infarct expansion after LAD ligation. A typical Masson's trichrome pattern in hearts transplanted with control, cardiac fibroblast, or CDCs is shown in Fig. 2E–H. The positive red-stained regions (viable tissue) within the predominately blue-stained regions (fibrous tissue) are the typical pattern seen in all hearts. Hearts receiving transplanted ESHF derived CDCs had significantly smaller infarct zone than hearts treated with media alone (control), cardiac fibroblasts or CHD derived CDCs (ESHF, n=7: 28.8±1.6% vs CNT, n=7: 46.3±1.8%, $P<0.0001$; vs Cfb, n=3: 44.9±2.5%, $P<0.001$; vs CHD, n=5: 38.8±2.9% $P<0.05$, Fig. 2I).

Physiological measurements consistently demonstrated a greater ability of the ESHF derived cells to improve cardiac function. One potential mechanism of cardiac recovery is the ability of both ESHF derived CDCs and CHD derived CDCs to differentiate into mature cardiomyocytes but at different rates due to their differences in the number of c-kit$^+$ CSCs, Sca-1$^+$ and ISL-1$^+$ cells. Using immunofluorescence to detect human nuclei, we observed low engraftment (<0.05%) of transplanted ESHF derived CDCs and CHD derived CDCs into cardiomyocytes in the peri-infarct of lateral infarct wall of rodent myocardium after 28 days (supporting information Fig. S4). Immunophenotypic characterization showed that the engrafted ESHF derived CDCs stained positive for cTNT and displayed mature cardiomyocyte characteristics. This low number of engrafted CDCs not only implies that the extent of differentiation of CDCs *in vivo* cannot account for the observed preservation of cardiac function but also other mechanisms must account for the increased functional capacity of ESHF derived CDCs. Furthermore, the increased number of CSCs within the ESHF derived CDCs did not allow detection of more CDC derived cardiomyocytes *in vivo*.

The ability of ESHF derived CDCs to promote cardiac repair may be due in part to increased production of secreted cytokine factors which trigger preservation of cardiomyocytes or formation of arterioles and neovessels, proliferation of endogenous cardiac stem cells or induction of resident cardiomyocyte proliferation. The frequency of cardiomyocytes co-expressing Ki-67$^+$ and α-sarcomeric actin (per mm^2) were increased after transplanting ESHF derived CDCs compared to CHD derived CDCs (ESHF: n=5, 0.7±0.12 vs CHD, n=4, 0.2±0.09, $P=0.03$ Fig. 3A–C) and were found only in the peri-infarct region. The endogenous c-kit$^+$ cells spanned the infarct and peri-infarct regions near the injected sites, which were significantly increased in the transplanted ESHF, derived CDCs (ESHF: n=4, 3.7±0.3 vs CHD, n=4, 2.2±0.4, $P=0.04$, Fig. 3D–F). Transplanted ESHF derived CDCs also augmented the preservation/formation of neovessels (isolectin B4) and arterioles (α-SMA) compared to CHD-derived CDCs (IB4: ESHF, n=5, 6.4±1.3 vs CHD, n=5, 2.8±0.8, $P=0.043$ and α-SMA: ESHF, n=3, 16.33±2.7 vs CHD, n=3, 7.0±1.0, $P=0.033$ Fig. 3G–L). Although blood vessels spanned the length of the infarct, the largest significant differences were found in the epicardium of the mid-infarct receiving the transplanted ESHF derived CDCs.

Unique Secretome of CDCs

Paracrine mechanisms may explain many of the beneficial effects of CDC transplantation. We have previously demonstrated the superior regeneration of neonatal derived hCDCs

when compared to adult derived CDCs due to increased level of key secreted cytokines which results in enhanced neovessel formation. Consistent with these results, we assayed expression levels of various key cytokines using quantitative RT-PCR expressed by the ESHF derived CDCs and CHD derived CDCs exposed to 16 hours of anoxia to stimulate an ischemic condition. Expression of VEGF-A (ESHF, n=5, 1.97±0.1 vs CHD, n=5, 0.6±0.1, *P*=0.02), SDF-1α (ESHF, n=5, 3.1±0.7 vs CHD, n=4, 1.0±0.15, *P*=0.019) and HIF-1α (ESHF, n=5, 1.4±0.16 vs CHD, n=5, 0.8±0.1, *P*=0.032) showed significant differences in the ESHF derived CDCs compared to CHD derived CDCs that suggest augmented secretion of pro-angiogenic factors (Fig. 4A–C). The cytokine expression of bFGF, IGF-1, IL-8, PDGF-A, CXCL-1, bFGF, and OSGIN1 did not reach a significant difference between the two groups (Fig. 4D–I). To further verify that the significant expression of VEGF-A and SDF-1α resulted in increased protein secretion, we analyzed the secretion of these paracrine factors from CHD-derived CDCs and ESHF derived CDCs. As shown in supporting information (Fig. S5), the secretion of VEGF-A and SDF-1α was significantly higher from ESHF derived CDCs as compared to CHD derived CDCs (*P*= 0.0173, *P*= 0.0043, respectively). We further evaluated the pro-angiogenic potency of the CDCs using an *in vitro* endothelial cell tube-forming assay using human umbilical vein endothelial cells (HUVECs). HUVECs cultured with endothelial growth media formed tubes within 6 hours while tube formation was diminished in presence of basal media not containing pro-angiogenic growth factors (Fig. 4J). Conditioned media from ESHF derived CDCs formed more significant mature endothelial tubes than conditioned media from CHD derived CDCs (ESHF, n=5, 3099±200 vs CHD, n=5, 1537±210, vs. Cfb, n=5, 1204±303, *P*=0.0081) by quantitative analysis of tube formation.

Increased heat shock response elevates functional recovery and cytokine secretion

Since the HSR is elevated in ESHF myocardium and stimulates cytokine secretion in other stem cells, (28–31) we next determined whether the HSR may play a role on the functional activity of the CDCs by initially establishing their expression pattern in the ESHF and CHD myocardium. Expression of HSF-1, the HSF master transcriptional activator, was up regulated in ESHF myocardium when compared to CHD myocardium, which also correlated with the activation of the downstream genes HSP60 and HSP70 (HSF-1: ESHF, n=4, 0.62±0.1 vs. CHD n=5, 0.33±0.064, *P*=0.031; HSP60: ESHF, n=4, 32.96±3.99 vs. CHD, n=5, 8.441±2.46, *P*=0.0159; HSP70: ESHF, n=4, 0.94±0.11 vs. CHD, n=5, 0.32±0.04, *P*=0.0159, Fig. 4K–M).

To determine whether the HSR triggered biochemical changes on the CDCs and could directly stimulate the CDCs to secrete higher levels of cytokines in gain of function experiments, we treated CHD derived CDCs with a well-known heat shock activator, celastrol (CEL) at an optimal concentration of 300nM for activation of Hsp70, Hsp27 (supporting information Fig. S6) (32). First, we determined the effect of the HSR on cell viability, apoptosis and proliferation. Induction of HSR significantly increased the CHD derived CDCs' cell proliferation and cell viability but no effect was observed on apoptosis (supporting information Fig. S7). We next studied whether the HSR stimulates the low cytokine producing CHD derived CDCs into higher cytokine producing CDCs by CEL or HS treatment. Conditioned media was collected from CHD derived CDCs after treatment

with heat shock (HS) or CEL. Both CEL and HS treatment significantly increased the secretion of SDF-1α (CHD, n=6, 468±28 vs CHD+CEL, n=6, 740±35, *P*=0.0036; vs CHD +HS, n=6, 679±41, *P*=0.022), VEGF-A (CHD, n=6, 70±6: vs CHD+CEL, n=6, 142±9, *P*=0.001; vs. CHD+HS, n=6, 87±11, *P*=0.04), PGDF-A (CHD, n=6, 1.3±0.3 vs CHD+CEL, n=6, 4.4±1.0, *P*=0.008; vs. CHD+HS, n=6, 4.4±1, *P*=0.03), IL-6 (CHD, n=6, 2247±100 vs CHD+CEL, n=6, 3393±290, *P*=0.016; CHD+HS, n=6, 3658±420, *P*=0.017) and FGF-2 (CHD, n=6, 49.16±5.8 vs CHD+CEL, n=6, 82.84±8.82; *P*=0.027; vs CHD+HS, n=6, 54.41±6.25, *P*>0.05) but no differences were seen in this analysis for IL-1, SCF, IGF-1, HGF and LIF (Fig. 5A–J). We further evaluated the pro-angiogenic potency of the CHD derived CDCs derived treated with HS or CEL using the in vitro endothelial cell tube-forming assay (Fig. 5K). The conditioned media from HS or CEL treated CHD derived CDCs significantly increased endothelial tube length when compared to conditioned media from CHD derived CDCs alone (CHD, n=5, 2602±303 vs CHD+CEL, n=5, 5582±882, *P*=0.041; vs CHD+HS n=5, 5578±400, *P*=0.022). We next analyzed the effect of the HSR on the expression of cardiovascular commitment/differentiation genes in HS or CEL treated CHD derived CDCs. Quantitative PCR showed that the HSR failed to trigger differentiation and expression of the cardiovascular commitment/differentiation genes in the HS or CEL treated CHD derived CDCs (supporting information Fig. S10). To determine whether the increased cytokine secretion correlated with increased functional potential of the CDCs, we performed a randomized blinded study to evaluate the functional effectiveness of transplanted CHD derived CDCs modified with the HS or CEL to preserve infarcted myocardium in our established acute MI rodent model. Baseline echocardiograms showed comparable cardiac function before MI for each group. Echocardiography performed after LAD ligation revealed increased left ventricle ejection fraction in rats transplanted with CHD derived CDCs that were treated with HS or CEL in comparison to untreated CHD derived CDCs and also controls at post-operative day 7 (CHD+CEL, n=4, 67.50±2.35% and CHD+HS, n=4, 62.18 ±2.7%; vs CHD, n=5: 42.34± 4.9%, *P*<0.0001 vs Control, n=6: 30.64 ± 6.21% *P*<0.0001) and at day 28 (CHD+CEL, n=4, 64.43±2.9% and CHD+HS, n=4, 62.78 ±4.81%; vs CHD, n=5: 41.3± 6.1%, *P*<0.0001 vs Control, n=6: 29.96 ± 6.1% *P*<0.0001, Fig. 5L). CHD derived CDCs treated with HS or CEL even outperformed the ESHF derived CDCs to functionally recover the MI myocardium at 7 days (ESHF, n=6: 53.18± 4.65%; vs CHD+CEL, *P*<0.001 and CHD+HS, *P*>0.05) and at 28 days (ESHF, n=6: 51.72± 6.63%; vs CHD+CEL, *P*<0.01 vs CHD+HS, *P*<0.05, Fig. 5L). The functional recovery correlated with increased preservation or formation of arterioles in the myocardium transplanted with CHD derived CDCs treated with HS or CEL when compared to untreated CHD derived CDCs (CHD, n=4, 2.25±0.9 vs CHD+CEL, n=4, 10.5±1.8, *P*=0.004; vs CHD+HS, n=4, 12.0±1.9, *P*=0.003, Fig. 5M). Taken together, these gain of function studies indicated that the HSR enhances the function of the transplanted low functioning CHD derived CDCs in the infarcted myocardium by possibly increasing cytokine secretion.

Loss of function of the heat shock response reduces functional recovery

We next performed loss of function studies to determine the effect of the HSR on the strongly performing ESHF derived CDCs. We inhibited the expression of HSF-1 in the ESHF derived CDCs using small interfering RNA (siRNA) targeting HSF-1, the master transcriptional regulator of the HS (Fig. 6A). Quantitative rt-PCR demonstrated effective

silencing of the HSF-1 (<5% expression) as compared to scrambled siRNA transfection (*P*=0.0286, Fig. 6B), which correlated with decreased Hsp70 RNA levels (*P*=0.0286, Fig. 6C). The effect of HSF-1 knockdown in ESHF-derived CDCs was analyzed for cell viability, apoptosis and proliferation. Knock down of HSF-1 adversely affected the cell viability and proliferation but not cell apoptosis (supporting information Fig. S8). Immunoblot analysis demonstrated that the inhibition of HSF-1 protein caused decreased expression of VEGF-A protein in the ESHF derived CDCs (Fig. 6D). To further determine the effect of HSF-1 inhibition on other secreted proteins, we collected the conditioned media from the ESHF derived CDCs either treated with siRNA targeting HSF-1 or scrambled siRNA control. Conditioned media from ESHF derived CDCs treated with siRNA targeting HSF-1 when compared to conditioned media from scrambled siRNA had significantly decreased secretion of VEGF-A (ESHF, n=5, 91±7 vs ESHF-HSF-KD, n=5, 42±11; *P*=0.03), SDF-1α (ESHF, n=5, 978±70: vs ESHF-HSF-KD, n=5, 470±80, *P*=0.0043), ANG-2 (ESHF, n=5, 796±64, vs ESHF-HSF-KD, n=6, 145±29, *P*=0.016), PGDF-A (ESHF, n=5, 15±2.3 vs ESHF-HSF-KD, n=5, 3.8±1.0, *P*=0.008) and FGF-2 (ESHF, n=5, 131±12 vs ESHF-HSF-KD, n=6, 75±9, *P*=0.006) but no differences in HGF-1, IGF-1, SCF, IL-1 and LIF levels were observed (Fig. 6E–J, supporting information Fig. S9). Since there was a decrease of many essential cytokines, we further evaluated the pro-angiogenic potency of the ESHF derived CDCs treated with siRNA targeting HSF-1 when compared to scrambled siRNA using the in vitro endothelial cell tube-forming assay (Fig. 6K). The conditioned media from ESHF derived CDCs treated with siRNA targeting HSF-1 significantly decreased HUVEC tube formation compared to conditioned media from ESHF derived CDCs treated with control scrambled siRNA (ESHF, n=5, 5410±1249 vs. ESHF-HSF-KD, n=5, 1537±257, *P*<0.0001). We next analyzed the effect of HSR on the expression of cardiovascular commitment/differentiation genes in HSF-1 knock down in ESHF derived CDCs. Quantitative PCR showed that reduced HSR did not change the amount of cardiovascular commitment/differentiation gene expression in HSF-1 knock down in ESHF derived CDCs (supporting information Fig. S10). We next tested whether HSF-1 knocked down ESHF derived CDCs had subsequently reduced ability to functionally recovery the myocardium in the MI rodent model due to the decreased cytokine secretion. Treatment of infarcted hearts with ESHF derived CDCs after HSF-1 knockdown (Fig. 6L) had decreased left ventricle function when compared to transplanted ESHF derived CDCs treated with scrambled siRNA at 7 days (Control, n=5, 49.63 ± 5.1% vs. ESHF, n=5, 66.59± 2.1%, *P*<0.001; vs ESHF-HSF-KD; n=4: 52.79 ±3.9%, *P*<0.01) and at 28 days (Control, n=5, 40.22 ± 5.4% vs ESHF, n=5, 64.20± 3.0% *P*<0.001; vs ESHF-HSF-KD, n=4, 49.18±1.55%, *P*<0.01). Furthermore, although there is a difference between the ESHF derived CDC study group's absolute calculated EF at baseline and in the controls at 7 and 28 days between the three different studies (Figure 2A, 5L, 6L), there still remains a significant improvement in EF following treatment with ESHF derived CDCs when compared to controls in each study. Thus, the observed trend toward significant improvement with ESHF derived CDCs treated hearts remains present in all studies that make this result very significant despite two different rat surgeons performing all the MIs. At another level and using the reverse logic, these results with the injected ESHF derived CDCs were confirmed by two independent rat surgeons and showed a similar and significant trend to functional recovery, bringing added strength to the data. Taken together, these loss-of-function studies demonstrated the critical

role of the HSR is playing in the functional abilities of the ESHF derived CDCs both in their ability to recover the MI myocardium and secretion of cytokines.

HSR effect on CDCs and endogenous c-kit$^+$ CSCs

By both gain of function and loss of function HSR studies, we have demonstrated that the HSR affects the functional activity of the CDCs due to increased levels of cytokine secretion. Since we also showed an increase in the endogenous c-kit$^+$ CSC population by the transplanted ESHF derived CDCs (Fig. 3) and an increase in SDF-α secretion by the HSR treated CDCs *in vitro* (Fig. 4), we next determined whether the HSR caused proliferation of the c-kit$^+$ CSCs as another possible mechanism for increased functional recovery when analyzed both *in vitro*. To determine the effect of the HSR, we treated CDCs with CEL and determined the expression of c-kit$^+$ and heat shock proteins. We observed that CEL in a dose-dependent manner promoted an increased expression of Hsp70, Hsp27, c-kit$^+$ and Isl-1 protein as analyzed by immunoblots within CHD derived CDCs (supporting information Fig. S5). The specificity of celastrol activity was then analyzed in the presence of triptolide (TTD), a known inhibitor of HSF-1 transactivation and HSR, in quantitative immunoblot analysis. Immunoblot analysis of CDCs after CEL or HS treatment at 42°C for 4 hours followed by 24 hours of recovery at 37°C showed a significant increase in c-kit$^+$ and Hsp70 protein expression (supporting information Fig. S11). This up regulation of c-kit+ and hsp70 was suppressed in the presence of TTD. To differentiate whether the HSR increased c-kit$^+$ protein expression or stimulated proliferation of the c-kit$^+$ CSCs, CHD derived CDCs were treated in the presence of CEL and then quantified by FACS analysis. Treatment with CEL increased the number of c-kit$^+$ CSCs within the CHD-derived CDCs by 3 fold, which was significantly inhibited in the presence of TTD (supporting information Fig. S12). In another complementary experiment, HS or CEL also led to a significant 3-fold increase in Ki67 expression in CHD derived CDCs (CNT, n=5, 13.6±1.3% vs CEL, n=5, 33.8±4.4%, $P<0.05$; HS, n=5 30.4±3.5%, $P=0.008$, Fig. 7A). Since CDCs are comprised of many other cell types and the HSR may directly or indirectly affect c-kit$^+$ CSC proliferation, we next tested HSR on immuno-purified c-kit$^+$ hCSCs. After 48 hours of exposure, CEL or HS treatment increased the cell proliferation of c-kit$^+$ CSCs by approximately 25% in comparison to non-treated c-kit$^+$ CSCs as analyzed by MTS assay (CNT, n=6, 0.9±0.02 vs CEL, n=6, 1.1±0.1, $P<0.01$; CNT, n=6, 0.9±0.02 vs HS, n=6, 1.0±0.3%, $P<0.05$, Fig. 7B). Collectively, these results strongly indicate that the HSR activated either by HS or CEL, triggered c-kit$^+$ CSC proliferation *in vitro* and that CEL was equivalent in activating the HSR when compared to physical heat shock.

Since we have shown that the HSR is critical for proliferation of c-kit$^+$ CSC population, we hypothesized that HSR should elevate the number of c-kit$^+$ CSCs in the native ESHF myocardium. We have previously shown that the number of c-kit$^+$ CSCs is the highest in the RAA compared to other chambers of the ESHF myocardium and so we have focused our studies on myocardial samples from the RAA. (12) Quantitative rt-PCR analysis of RAA biopsies determined that the c-kit$^+$ expression was significantly higher in ESHF myocardium as compared to CHD myocardium (CHD, n=4, 0.0525±0.044 vs. ESHF, n=4, 0.107±0.013, $P= 0.0265$, Fig. 7C). Immunohistochemical staining of myocardial sections directly obtained from the RAA biopsies revealed that c-kit$^+$ CSCs were among and closely opposed to the α-

sarcomeric actin^{+} cardiomyocytes (Fig. 7D). There was no statistical differences in the number of c-kit^{+} CSCs between infants and children in ESHF myocardium which is in contrast to our previously reported finding which showed a decrease in number of c-kit^{+} CSCs with advancing age seen in CHD patients with normal myocardium (infants, n=5, 8.66±1 vs children, n=7, 7.1±0.6, *P*=0.2) (12). The number of c-kit^{+} CSCs present in the ESHF myocardium from infants and children was similar to our previously published number of c-kit+ CSCs present in the neonatal myocardium (8.9±0.4%). These results demonstrated that the ESHF myocardium increases the number of c-kit^{+} CSCs to a level similar to normal neonatal myocardium.

Discussion

We demonstrated that isolated and ex vivo expanded pediatric ESHF derived CDCs were more efficacious compared to CDCs derived from CHD hearts (VSD hearts or DNR hearts) when transplanted into ischemic rodent myocardium. This augmented functional recovery was mediated in part by increased secretion levels of SDF-1α and VEGF-A, which increased angiogenesis, increased the number of CSCs, and increased proliferation of intrinsic native cardiomyocytes. We showed three lines of evidence that HSR is the key regulator that enhances the CDCs' functional activity through the activation of a more effective secretome. These findings suggest that not all CDCs derived from the heart are functionally similar. In fact, the functional ability of the CDCs is related to the physiological state of the heart. Thus, more severely decompensated hearts may afford more highly potent CDCs for therapeutic administration secondary to a more robustly up regulated HSR and secretome in this patient population.

We derived CDCs from ESHF myocardium and initially compared their *in vitro* characteristics and functional potency to CDCs derived from CHD hearts that either have normally functioning myocardium despite having a structural cardiac defect, a VSD, or from donor hearts at the time of heart transplantation also having normal functioning myocardium. Our findings highlight the following main points. First, we demonstrated that all CDCs were easily isolated irrespective of the cardiac source. The CDCs derived from either ESHF or CHD myocardium had a very similar cellular morphology and growth potential (Fig. 1A, B). Secondly, the ESHF derived CDCs had an increased number of c-kit^{+}, Sca-1^{+}, and ISL-1^{+} cells in comparison to CHD derived CDCs but the reason for this increased number of CSCs is unclear. One explanation is that CDCs derive their cellular composition from the tissue of origin as is seen in studies with neurospheres and in our previously published characterization of neonatal derived CDCs (33, 34). Our results are consistent with this notion since the ESHF myocardium consistently had elevated numbers of endogenous cardiac stem cells when compared to CHD myocardium (Fig. 7D). Lastly, we examined the paracrine factors that are currently viewed to be the main mechanism of functional recovery by transplanted CDCs due to minimal observed engraftment and terminal differentiation to mature cardiac phenotypes (35, 36). The ESHF derived CDCs produced higher levels of SDF-1α and VEGF-A and thus promoted superior endothelial tube length (Fig. 4A–C, J). Furthermore, the HSR boosted the functional activity of the CHD derived CDCs by stimulating the production of SDF-1α and VEGF-A, amongst other cytokines and this correlated with stronger functional recovery within the infarcted

myocardium (Fig. 5A, 5B, 5L). Our results are consistent with a recently reported study that demonstrated elevated secreted levels of SDF-1α in adult heart failure derived CDCs when compared to CDCs derived from healthy donors or from acute MI patients (20). This study, however, failed to show a difference in the cellular composition of CDCs between these donor groups, which is in contrast to our results where there was a significant increase in c-kit$^+$, Sca-1$^+$ and Isl-1$^+$ cells in the ESHF derived CDCs (Fig. 1C&J). The reason for this discrepancy maybe explained by the age of the ESHF hearts. The mechanism underlying the elevated SDF-1α by the ESHF derived CDCs were never explored in this previous study, but our data strongly suggests that the HSR is a powerful pathway governing the secretome of the CDCs. These data taken together along with the lack of engrafted cells suggest the critical role of the secretome to functionally recover the infarcted myocardium by transplanted CDCs, particularly ESHF derived CDCs.

One of our novel finding is that the HSR pathway critically regulates the secretome within CDCs. We provided three lines of evidence that the key pathway triggered by the HSR is essential for the functional recovery by the CDCs. First, we demonstrated that the low functioning CHD derived CDCs when treated either by celastrol or HS secreted higher levels of cytokines and thus recovered more of the MI myocardium. Secondly, we showed in loss of function studies that ESHF derived CDCs treated with siRNA targeting HSF-1 had reduced ability to recover the ischemic myocardium due to decreased levels of cytokine secretion. Lastly, we showed that the HSR by itself can enhance the proliferation of CDCs and c-kit$^+$ CSCs *in vitro*. The exact mechanism of how the HSR stimulates this elevated cytokine secretome is likely multifactorial. Several plausible mechanisms include the following. Firstly, HSF-1 may directly trans-activate key regulators that control cytokine secretion, including HIF-1α. Previous studied have shown that modified mesenchymal stem cells with overexpression of HSP27, had increased recovery of the injured myocardium through elevated VEGF-A secretion which implicates the HIF-1α pathway (37). Secondly, the HSR may cause increased exosomes production that may directly affect the local ischemic cardiomyocyte environment. This mechanism has been recently reported in rodent cardiac derived Sca-1$^+$ cells that were treated with the HSR (38). They further showed the critical role of the HSF1/miR34a/HSP70 pathway in secreting exosomes to recover the ischemic myocardium. Finally, the HSR may stimulate increased cytokine production through an unknown mechanism that maybe uncovered through a miRNA or a gene expression discovery study. We are actively pursuing these potential mechanisms to determine how the novel HSR pathway regulates the cytokine production in the CDCs.

Our study demonstrated that the HSR stimulated by a small molecule, celastrol, strongly enhanced the function of CDCs by regulating their secretome. Celastrol may have some clear advantages in optimizing cell-based therapy. First, this approach does not contain a multi-component mixture of factors but only a single factor activating a single pathway. Secondly, this approach enhances the secretion of pro-angiogenic factors that can increase functional myocardial recovery. Last, celastrol has been shown to have anti-apoptotic and anti-inflammatory activity, (39, 40) a low side-effect profile, and the ease of oral administration. These data support the novel biological activity of celastrol and the direct

impact on improving the potential benefits of CDC based cell therapy, which relies on the innate cellular machinery.

Our data raises the question why the highly functional pediatric ESHF derived CDCs are unable to overcome their own dysfunctional myocardium. Several explanations may exist. First, despite that the isolated ESHF derived CDCs are highly functional, the endogenous CSCs may have altered functional ability due to oxidative and apoptotic stressors present in the dysfunctional myocardium. We have preliminary data that c-kit$^+$ CSCs derived from pediatric ESHF myocardium also display a superior functional ability to improve the infarcted myocardium in the MI rodent. Second, these results suggested that ESHF derived CDCs may achieve their superior functional activity by raising their total number of CSCs within the CDC population. We have similarly reported that neonatal derived CDCs had an increased number of c-kit$^+$ and Isl-1$^+$ cells that correlated with improved functional recovery of the ischemic myocardium and thus out-performed adult derived CDCs in this comparative analysis (15). Last, one can make the reverse argument that if the highly functional ESHF derived CDCs were not present in the failing myocardium, then the myocardium would have deteriorated at a faster rate since there is increased apoptosis and oxidative stress in the failing heart (18). Further studies will be needed to elucidate the importance of the functional capacity of the ESHF derived CDCs in the failing myocardium.

There are substantial gaps in our knowledge on how to optimize CDC based cell therapy for heart disease. Multiple factors can prevent the CDCs from functioning at their full potential, one of which is the dysregulation of the secretome. Another impediment is the survival rate of the transplanted CDCs. A cocktail of pro-survival factors inhibiting potential death pathways have been used previously to improve the functional recovery by transplanted cardiomyocytes derived from human embryonic stem cells (42). Last, patient characteristics may influence CDCs to perform at their maximum ability when injected into the ischemic myocardium. In conclusion, our results indicate that CDCs derived from pediatric ESHF myocardium are highly functional. The enhanced functional recovery is due to a potent secretome. Lastly, we uncovered the HSR pathway as a novel mechanism that regulates the secretome. These results may have broad applications to optimize cardiac stem cell protocols in the future.

Supplementary Material

Refer to Web version on PubMed Central for supplementary material.

Acknowledgments

We thank Dr. Carl Backer for the procurement of the heart tissues.

Sources of Funding

This work was supported by the following grants: National Institutes of Health (KO8HL097069 and R01HL118491), the Thoracic Surgical Foundation for Research and Education, and Children's Heart Foundation.

References

1. Roger VL. Epidemiology of heart failure. Circ Res. 2013; 113:646–659. [PubMed: 23989710]

2. Go AS, Mozaffarian D, Roger VL, et al. Heart disease and stroke statistics-2014 update: a report from the american heart association. Circulation. 2014; 129:e28–e292. [PubMed: 24352519]

3. Rossano JW, Kim JJ, Decker JA, et al. Prevalence, morbidity, and mortality of heart failure-related hospitalizations in children in the United States: a population-based study. Journal of cardiac failure. 2012; 18:459–470. [PubMed: 22633303]

4. Porrello ER, Mahmoud AI, Simpson E, et al. Transient regenerative potential of the neonatal mouse heart. Science. 2011; 331:1078–1080. [PubMed: 21350179]

5. Messina E, De Angelis L, Frati G, et al. Isolation and expansion of adult cardiac stem cells from human and murine heart. Circulation research. 2004; 95:911–921. [PubMed: 15472116]

6. Beltrami AP, Barlucchi L, Torella D, et al. Adult cardiac stem cells are multipotent and support myocardial regeneration. Cell. 2003; 114:763–776. [PubMed: 14505575]

7. Smith R, Pawlicki R, Kokai I, et al. Navigating in a shape space of registered models. IEEE transactions on visualization and computer graphics. 2007; 13:1552–1559. [PubMed: 17968109]

8. Matsuura K, Nagai T, Nishigaki N, et al. Adult cardiac Sca-1-positive cells differentiate into beating cardiomyocytes. The Journal of biological chemistry. 2004; 279:11384–11391. [PubMed: 14702342]

9. He JQ, Vu DM, Hunt G, et al. Human cardiac stem cells isolated from atrial appendages stably express c-kit. PloS one. 2011; 6:e27719. [PubMed: 22140461]

10. Smith RR, Barile L, Cho HC, et al. Regenerative potential of cardiosphere-derived cells expanded from percutaneous endomyocardial biopsy specimens. Circulation. 2007; 115:896–908. [PubMed: 17283259]

11. Chimenti I, Gaetani R, Barile L, et al. Isolation and expansion of adult cardiac stem/progenitor cells in the form of cardiospheres from human cardiac biopsies and murine hearts. Methods in molecular biology. 2012; 879:327–338. [PubMed: 22610568]

12. Mishra R, Vijayan K, Colletti EJ, et al. Characterization and functionality of cardiac progenitor cells in congenital heart patients. Circulation. 2011; 123:364–373. [PubMed: 21242485]

13. Bu L, Jiang X, Martin-Puig S, et al. Human ISL1 heart progenitors generate diverse multipotent cardiovascular cell lineages. Nature. 2009; 460:113–117. [PubMed: 19571884]

14. Makkar RR, Smith RR, Cheng K, et al. Intracoronary cardiosphere-derived cells for heart regeneration after myocardial infarction (CADUCEUS): a prospective, randomised phase 1 trial. Lancet. 2012; 379:895–904. [PubMed: 22336189]

15. Simpson DL, Mishra R, Sharma S, et al. A strong regenerative ability of cardiac stem cells derived from neonatal hearts. Circulation. 2012; 126:S46–S53. [PubMed: 22965993]

16. Kajstura J, Leri A, Finato N, et al. Myocyte proliferation in end-stage cardiac failure in humans. Proceedings of the National Academy of Sciences of the United States of America. 1998; 95:8801–8805. [PubMed: 9671759]

17. Anversa P, Kajstura J. Ventricular myocytes are not terminally differentiated in the adult mammalian heart. Circulation research. 1998; 83:1–14. [PubMed: 9670913]

18. Rajabi M, Kassiotis C, Razeghi P, et al. Return to the fetal gene program protects the stressed heart: a strong hypothesis. Heart failure reviews. 2007; 12:331–343. [PubMed: 17516164]

19. Malliaras K, Makkar RR, Smith RR, et al. Intracoronary cardiosphere-derived cells after myocardial infarction: evidence of therapeutic regeneration in the final 1-year results of the CADUCEUS trial (CArdiosphere-Derived aUtologous stem CElls to reverse ventricULar dySfunction). Journal of the American College of Cardiology. 2014; 63:110–122. [PubMed: 24036024]

20. Cheng K, Malliaras K, Smith RR, et al. Human cardiosphere-derived cells from advanced heart failure patients exhibit augmented functional potency in myocardial repair. JACC. Heart failure. 2014; 2:49–61. [PubMed: 24511463]

21. Bolli R, Chugh AR, D'Amario D, et al. Cardiac stem cells in patients with ischaemic cardiomyopathy (SCIPIO): initial results of a randomised phase 1 trial. Lancet. 2011; 378:1847–1857. [PubMed: 22088800]

22. Zaruba MM, Soonpaa M, Reuter S, et al. Cardiomyogenic potential of C-kit(+)-expressing cells derived from neonatal and adult mouse hearts. Circulation. 2010; 121:1992–2000. [PubMed: 20421520]

23. Simpson D, Liu H, Fan TH, et al. A tissue engineering approach to progenitor cell delivery results in significant cell engraftment and improved myocardial remodeling. Stem Cells. 2007; 25:2350–2357. [PubMed: 17525236]
24. Chimenti I, Smith RR, Li TS, et al. Relative roles of direct regeneration versus paracrine effects of human cardiosphere-derived cells transplanted into infarcted mice. Circulation research. 2010; 106:971–980. [PubMed: 20110532]
25. Zhang X, Wang X, Zhu H, et al. Hsp20 functions as a novel cardiokine in promoting angiogenesis via activation of VEGFR2. PloS one. 2012; 7:e32765. [PubMed: 22427880]
26. Miyata S, Minobe W, Bristow MR, et al. Myosin heavy chain isoform expression in the failing and nonfailing human heart. Circ Res. 2000; 86:386–390. [PubMed: 10700442]
27. Razeghi P, Young ME, Alcorn JL, et al. Metabolic Gene Expression in Fetal and Failing Human Heart. Circulation. 2001; 104:2923–2931. [PubMed: 11739307]
28. Afanasiev SA, Falaleeva LP, Rebrova TU, et al. Effect of stress-proteins on survival of bone marrow mesenchymal stem cells after intramyocardial transplantation against the background of postinfarction heart remodeling. Bulletin of experimental biology and medicine. 2008; 146:111–115. [PubMed: 19145366]
29. Genth-Zotz S, Bolger AP, Kalra PR, et al. Heat shock protein 70 in patients with chronic heart failure: relation to disease severity and survival. International journal of cardiology. 2004; 96:397–401. [PubMed: 15301893]
30. Wang Y, Chen L, Hagiwara N, et al. Regulation of heat shock protein 60 and 72 expression in the failing heart. Journal of molecular and cellular cardiology. 2010; 48:360–366. [PubMed: 19945465]
31. Stolzing A, Sethe S, Scutt AM. Stressed stem cells: Temperature response in aged mesenchymal stem cells. Stem cells and development. 2006; 15:478–487. [PubMed: 16978051]
32. Mu TW, Ong DS, Wang YJ, et al. Chemical and biological approaches synergize to ameliorate protein-folding diseases. Cell. 2008; 134:769–781. [PubMed: 18775310]
33. Reynolds BA, Weiss S. Generation of neurons and astrocytes from isolated cells of the adult mammalian central nervous system. Science. 1992; 255:1707–1710. [PubMed: 1553558]
34. Rietze RL, Reynolds BA. Neural stem cell isolation and characterization. Methods in enzymology. 2006; 419:3–23. [PubMed: 17141049]
35. Mirotsou M, Jayawardena TM, Schmeckpeper J, et al. Paracrine mechanisms of stem cell reparative and regenerative actions in the heart. Journal of molecular and cellular cardiology. 2011; 50:280–289. [PubMed: 20727900]
36. Angelini A, Castellani C, Ravara B, et al. Stem-cell therapy in an experimental model of pulmonary hypertension and right heart failure: role of paracrine and neurohormonal milieu in the remodeling process. The Journal of heart and lung transplantation : the official publication of the International Society for Heart Transplantation. 2011; 30:1281–1293.
37. McGinley LM, McMahon J, Stocca A, et al. Mesenchymal stem cell survival in the infarcted heart is enhanced by lentivirus vector-mediated heat shock protein 27 expression. Human gene therapy. 2013; 24:840–851. [PubMed: 23987185]
38. Feng Y, Huang W, Meng W, et al. Heat shock improves Sca-1+ stem cell survival and directs ischemic cardiomyocytes toward a prosurvival phenotype via exosomal transfer: a critical role for HSF1/miR-34a/HSP70 pathway. Stem cells. 2014; 32:462–472. [PubMed: 24123326]
39. Kannaiyan R, Shanmugam MK, Sethi G. Molecular targets of celastrol derived from Thunder of God Vine: potential role in the treatment of inflammatory disorders and cancer. Cancer letters. 2011; 303:9–20. [PubMed: 21168266]
40. Salminen A, Lehtonen M, Paimela T, et al. Celastrol: Molecular targets of Thunder God Vine. Biochemical and biophysical research communications. 2010; 394:439–442. [PubMed: 20226165]
41. Cesselli D, Beltrami AP, D'Aurizio F, et al. Effects of age and heart failure on human cardiac stem cell function. The American journal of pathology. 2011; 179:349–366. [PubMed: 21703415]
42. Laflamme MA, Chen KY, Naumova AV, et al. Cardiomyocytes derived from human embryonic stem cells in pro-survival factors enhance function of infarcted rat hearts. Nature biotechnology. 2007; 25:1015–1024.

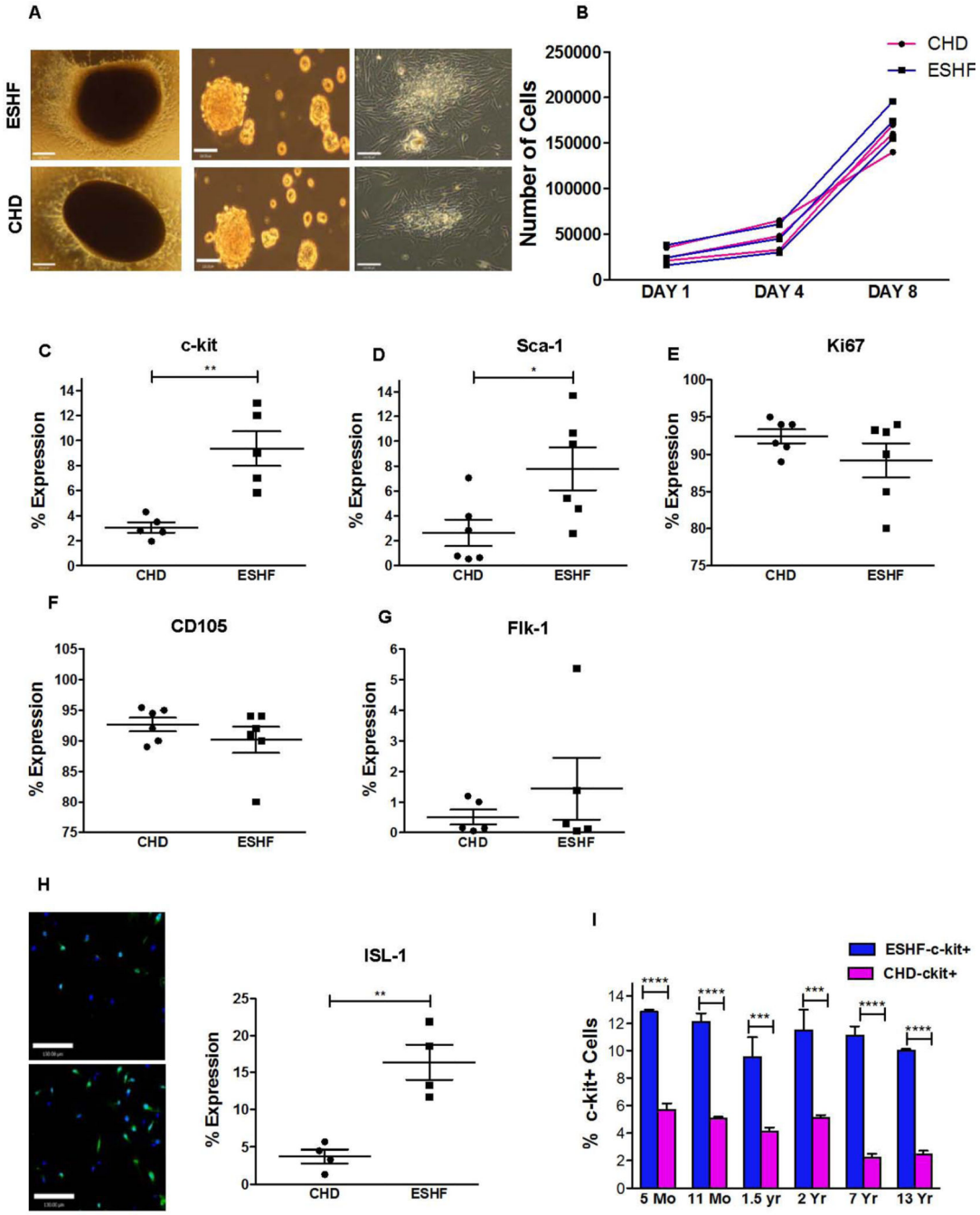

Figure. 1.

Characterization of ESHF and CHD derived CDCs. (**A,i–vi**) Generation of cardiospheres from RAA explant cultures. (i & iv) Adherent tissue explant present at one week. (ii & v) Phase-bright cells were removed and replated them in cardiosphere-growing medium–induced cardiosphere formation (iii & vi). Cardiospheres expanded to a monolayer of hCDCs (Scale bar = 120μm). **(B)** Population doubling over time between ESHF and CHD derived hCDCs was similar. **(C–G)** Antigenic phenotype of ESHF and CHD derived CDCs demonstrated higher expression of c-kit^{+} (**P=0.0079) and Sca-1 (*P=0.041) and not Ki67,

CD105, Flk-1. **(H)** Elevated ISL-1 expression was seen in ESHF derived CDCs when compared to CHD derived CDCs determined by immunofluorescence (***P*<0.01) (scale bar = 120μm). **(I)** A higher number of c-kit^{+} cells were present in ESHF derived CDCs than in CHD derived CDCs (****P*<0.0001, *****P*<0.0001). Data are analyzed by non-parametric t-test (Mann-Whitney's analysis) and presented as mean ± SEM.

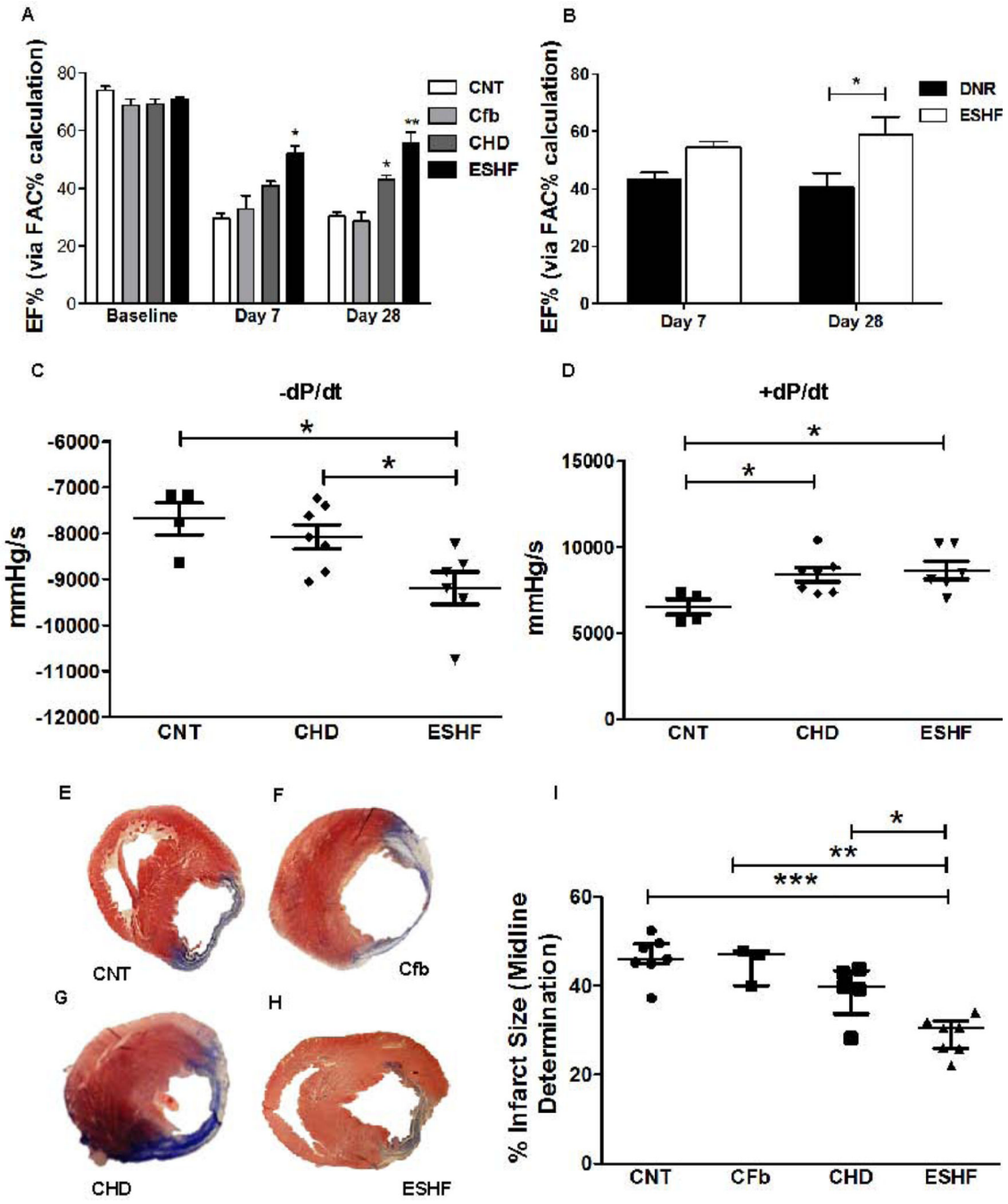

Figure. 2.

Transplanted ESHF derived CDCs outperformed CHD derived CDCs in preserving cardiac function after myocardial infarction in immunodeficient rats. Echocardiogram analysis was performed before and after surgery at day 7 days and day 28. **(A)** Left ventricle blood pool fractional area change in diastole (FAC, ejection fraction) was significantly improved in infarcted hearts transplanted with ESHF derived CDCs compared to transplanted CHD derived CDCs (*P<0.05), control (**=P<0.01), and Cfb (***P<0.001) at 7 and 28 days **(B)** As another age-matched cohort, CDCs derived from ESHF outperformed CDCs derived

from donor hearts (DNR) in the preserving left ventricle ejection fraction in the immunodeficient myocardial infarct model at 28 days (*P<0.05). **(C, D)** Transplanted ESHF derived CDCs and CHD derived CDCs significantly improved hemodynamics when compared to controls as measured by −dP/dt (*P<0.05) and +dP/dt (*P< 0.05). **(E–I)** Infarct size determined by Masson's trichrome staining was reduced with transplanted ESHF derived CDCs when compared with control (***=P<0.001), cardiac fibroblast (**=P<0.01), and CHD derived CDCs (*P<0.05). Data are analyzed by 2-Way ANOVA followed by Benferroni's analysis or one–way ANOVA (non-parametric, Kruskal-Wallis test) followed by Dunns analysis. Data are presented as mean ± SEM.

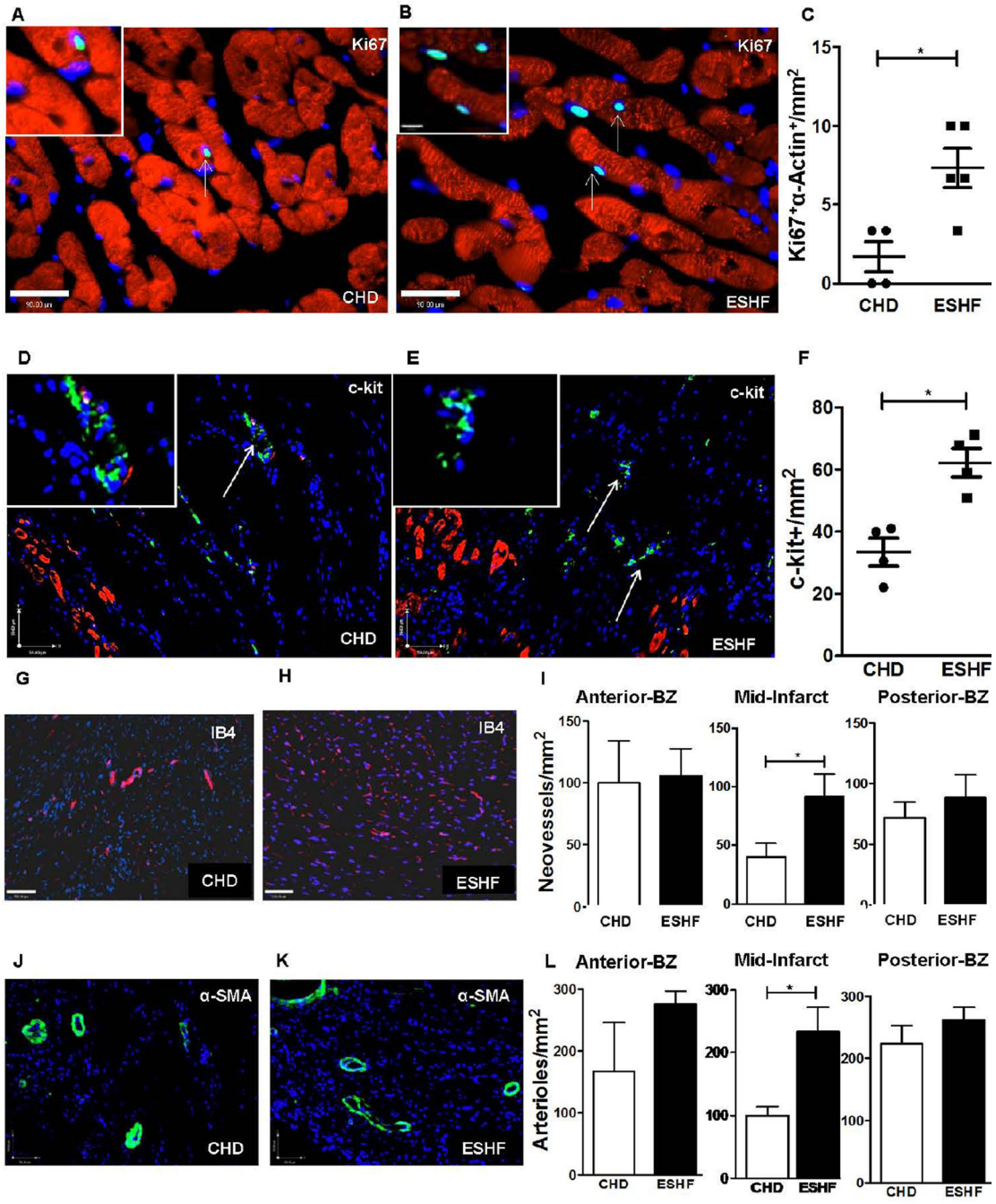

Figure. 3.

ESHF derived CDCs treatment enhanced cell cycle re-entry of cardiomyocytes, increased endogenous c-kit$^+$ cells and neovessel formation. **(A, B)** Immunofluorescence for Ki67 demonstrated increased cell cycle re-entry of sarcomeric α-actin$^+$ cardiomyocytes in hearts treated with CHD-derived CDC or ESHF-derived CDCs. (scale bar = 90μm). Arrow indicates towards proliferating cardiomyocytes. **(C)** ESHF derived CDCs promoted increased cell cycle re-entry of cardiomyocytes (*P=0.03). **(D, E)** Immunofluorescence showed increased number of endogenous c-kit$^+$ cells in myocardium treated with ESHF

derived CDCs in comparison to CHD derived CDCs within the border zone, typically as small niches (scale bar = 59μm). **(F)** A higher number of c-kit$^+$ cells were present in ESHF derived CDCs treated myocardium than treated with CHD derived CDCs (**P*=0.04). Immunofluorescence demonstrated increased formation of neovessels marked by IB4 expression **(G–I)** nad of arterioles marked by α-SMA expression (**J–L**) in myocardium sections of the mid-infarct regions transplanted with ESHF derived CDCs than transplanted with CHD derived CDCs (IB4: **P*=0.043 and α-SMA: **P* =0.033). Data are analyzed by non-parametric t-test (Mann-Whitney's analysis) and presented as mean ± SEM.

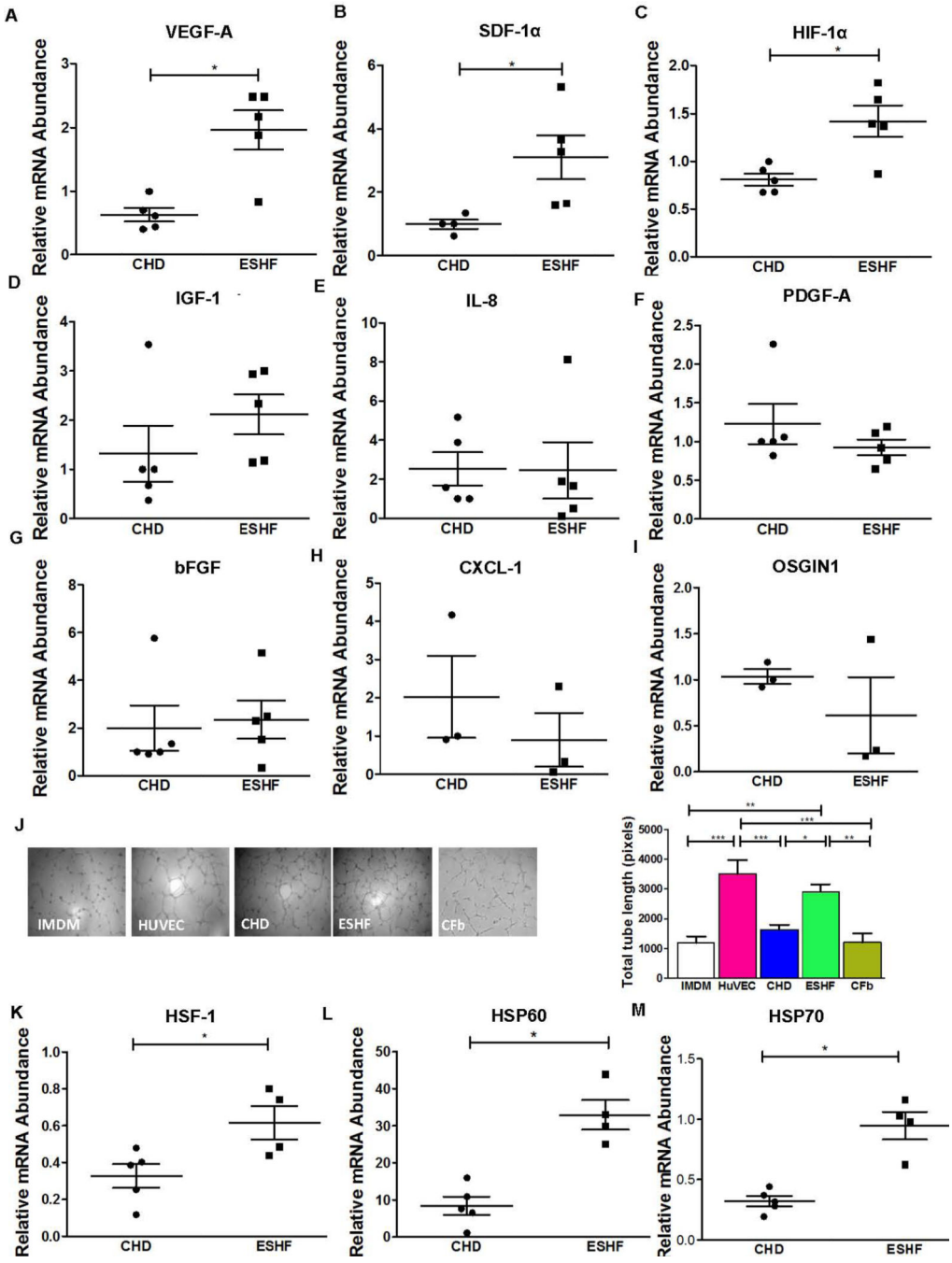

Figure. 4.

Enhanced cytokine expression by ESHF derived CDCs. Expression levels of several key cytokines were determined by RT-PCR after 16 hours of hypoxia. () ESHF derived CDCs showed up regulated expression of VEGF-1A (**P*=0.02), SDF-1α (**P*=0.019) and HIF-1α (**P*=0.032). (**D–I**) Expression for IGF1, IL-8, PGDFB, bFGF, CXCL1, and OSGIN1 did not show any significant difference between CHD and ESHF derived CDCs. To determine if the augmentation of pro-angiogenic factors in ESHF derived CDCs translated to increased vessel formation, *in vitro* endothelial cell tube-formation assay was performed using human

umbilical vein endothelial cells (HUVEC). (**J**) Representative images of HUVECs 8 hours after plating on matrix-coated wells in serum free basal medium (IMDM), HUVEC condition media, CHD derived CDCs condition medium and ESHF derived CDCs condition medium and cardio-fibroblast condition medium (Cfb). Quantification of total tube length demonstrated significantly increased tube length with ESHF derived CDCs as compared to CHD derived CDCs, IMDM and Cfb (scale bar = 140μm). (**=P<0.01 and ***=P<0.001 **(K–M)** Quantitative rt-PCR analysis of myocardial biopsies obtained from CHD or ESHF patients demonstrated increased HSF-1 (*P<0.05), HSP 60 (*P<0.05), and HSP 70 (*P<0.05) in ESHF myocardium. Data are analyzed one-Way ANOVA followed by Dunns analysis or non-parametric t-test followed by Mann-Whitney's analysis and presented as mean ± SEM.

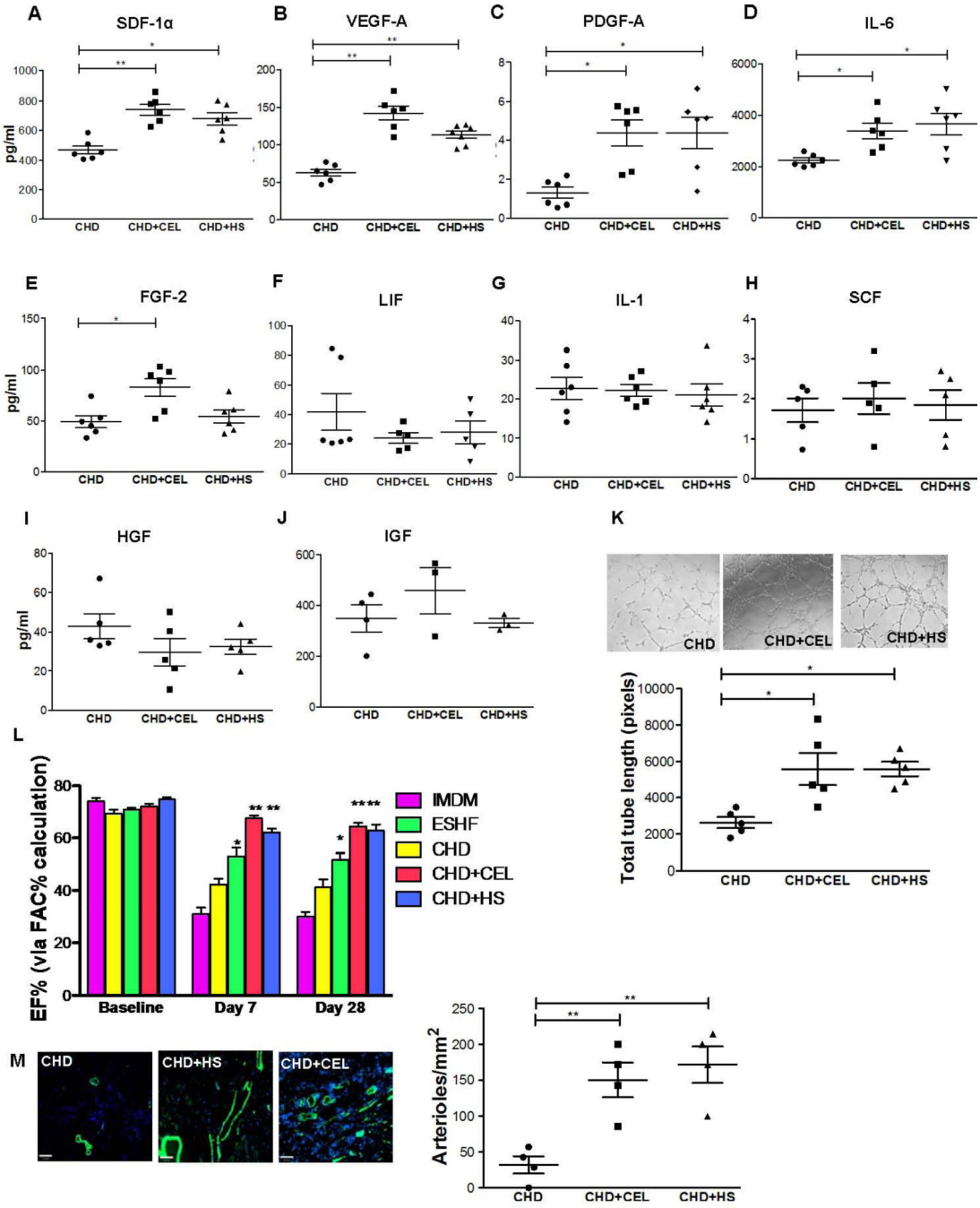

Figure. 5.

HSR promotes the angiogenic and myocardial repair potential of CHD derived hCDCs. CEL or HS treatment of CHD derived CDCs increased selective cytokine secretion as determined by ELISA on conditioned media after 72 hours of CEL or HS treatment. **(A–E)** In the presence of CEL or HS, CHD derived CDCs showed increased secretion of SDF-1α (**P*=0.022), VEGF-1A (**P*=0.04), PGDFB (**P*=0.03), IL-6 (**P*=0.017) and FGF-2 (**P*=0.027), **(F–J)** but not LIF, SCF, IGF1, HGF, LIF and IL-1. HSR enhanced the pro-angiogenic capacity of CHD derived CDCs. **(K)** Representative images (left) and

quantification of total tube length (right) of HUVECs 8 hours after plating on matrix coated wells with IMDM or condition media from HUVECs, CM-CHD, CM-CDCs-CEL and CM-CDCs-HS (scale bar = 140μm). **(L)** CEL treated CHD derived CDCs outperformed non-treated CHD derived CDCs in preserving left ventricle function in the infarction myocardium. Treated or untreated CDCs were injected into the infarcted myocardium of immunodeficient rats and function was assessed by echocardiography at 7 days and at 28 days **(M)** Immunofluorescence (left) demonstrated increased preservation/formation of arterioles (α-SMA, green) after HS or CEL treatment of CHD derived CDCs (right, $^{**}P<0.01$). Data are analyzed by 2-Way ANOVA followed by Benferroni's analysis or one –way ANOVA (non-parametric, Kruskal-Wallis test) followed by Dunns analysis. Data are presented as mean ± SEM.

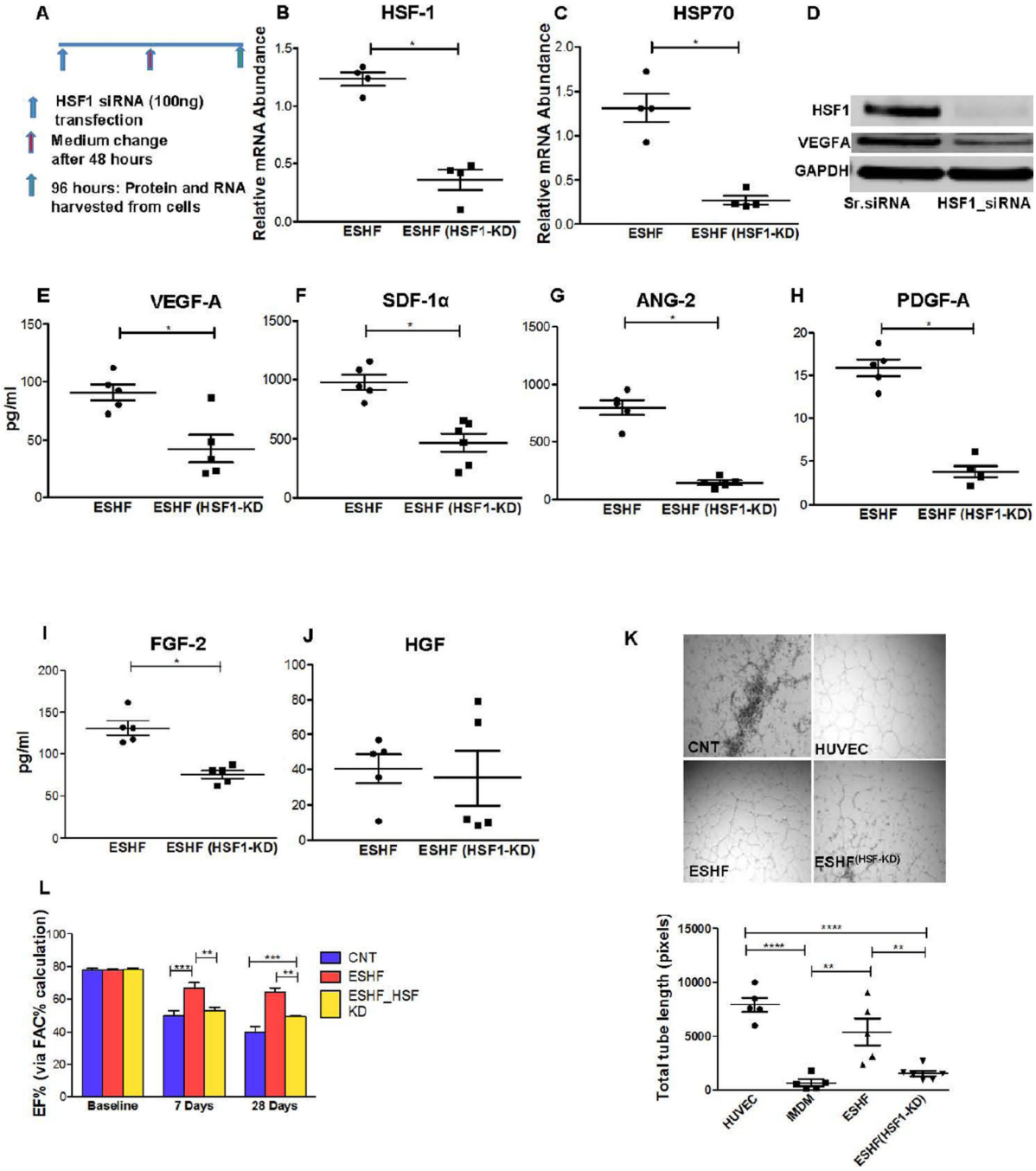

Figure. 6.

HSR plays a vital role in the functional potential of hCDCs. HSF-1 transcription factor was knock down (KD) using siRNA in ESHF derived CDCs (ESHF(HSF1-KD)). **(A)** Knockdown of HSF1 by siRNA, administration, and sample collection was performed as outlined. **(B–C)** HSF-1 and HSP70 expression was decreased to less than 5% expressed in ESHF (HSF1-KD). **(D)** HSF-1 KD reduced the expression of HSF-1 and VEGF-1A protein. **(E–I)** Secretion of paracrine factors was significantly reduced after HSF-1 knockdown in ESHF derived CDCs: VEGF-1A (P=0.03), SDF-1α (P=0.0043), PGDFB (P=0.008), ANG-2

(*P*=0.016) and FGF-2 (*P*=0.006) but no difference was seen for HGF. **(K)** Representative images of HUVEC tube formation (left) and quantification of total tube length (right) after plating HUVEC cells on matrix coated wells with IMDM condition medium from ESHF and ESHF (HSF1-KD) CDCs (scale bar = 100μm) (****=*P*<0.0001, ***=*P*<0.001, **=*P*<0.01). **(L)** Knockdown of HSF-1 in ESHF derived CDCs resulted in reduction of left ventricle ejection fraction as determined by echocardiography at 7 days and at 28 days.

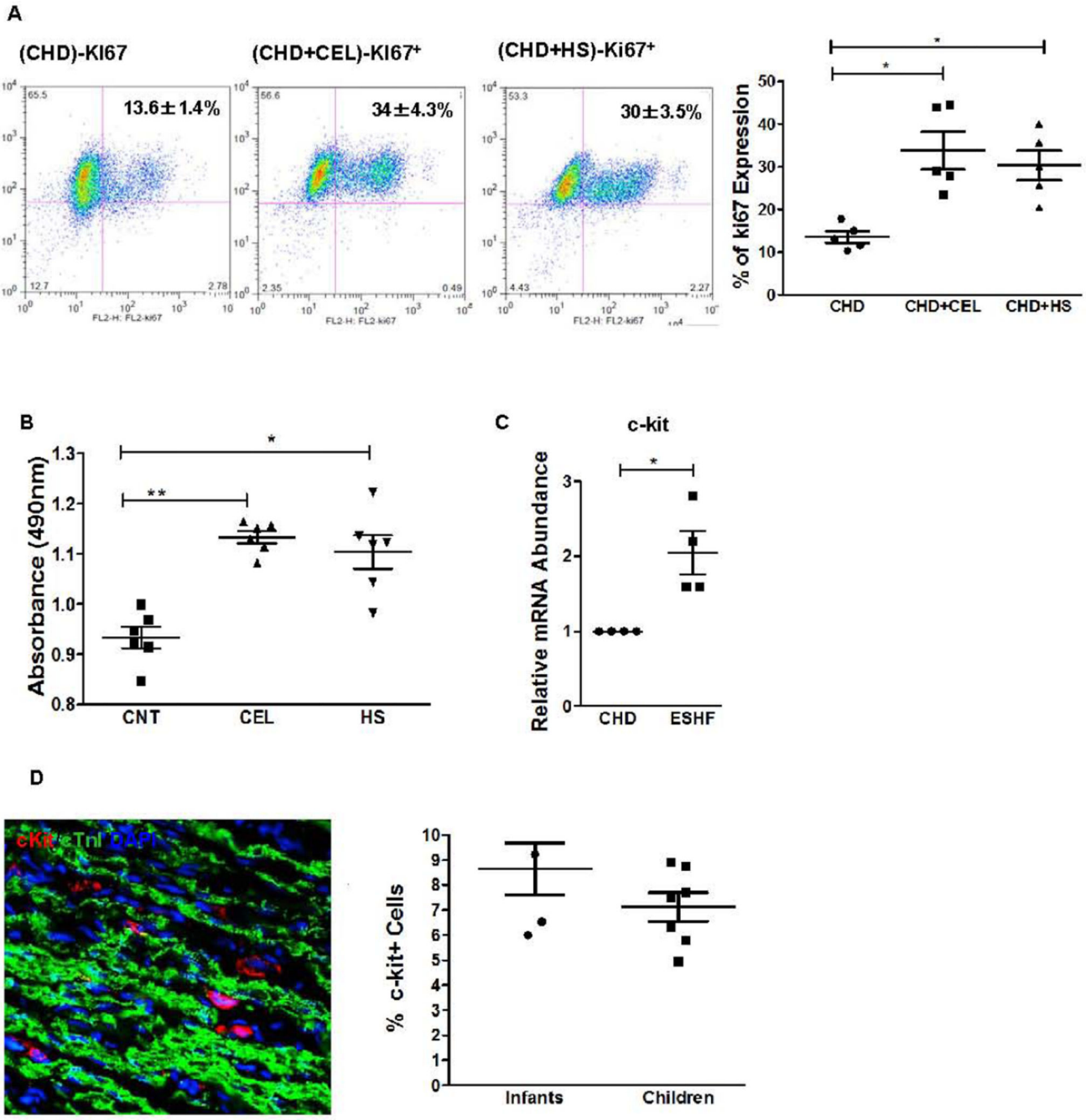

Figure. 7. Effect of HSR on CDCs and endogenous c-kit$^+$ CSCs

(A) Representative dot plot of FACS analysis for Ki67 expression of CHD derived CDCs after treatment with HS or CEL. Quantification (right) showed 3.0 fold increase in cell proliferation of the CEL or HS treated CDCs as compared to CNT (*P<0.05). **(B)** Effect of HSR on c-kit$^+$/CD45$^-$ hCSCs. HS or CEL treatment significantly increased cell proliferation of purified c-kit$^+$ CSCs as determined by MTS assay. **(C)**. Expression profile of cardiac specific stem cells markers in CHD and ESHF myocardium. Quantitative RT-PCR suggested a 2-fold increase in the c-kit$^+$ expression of ESHF myocardium as compared to

CHD myocardium. Data analyzed by non-parametric t-test followed by Mann-Whitney analysis. **(D)** The number of c-kit$^+$ CSCs were increased in ESHF myocardial sections as detected by confocal microscopy images with staining of c-kit$^+$ (red), cardiac TnI (green), and nuclear DAPI (blue). The results also indicate that the relative mean percentage of c-kit$^+$ CSCs did not vary across ages. Results are presented as mean of percentage of total cells per sample. Data are analyzed by 2-Way ANOVA followed by Benferroni's analysis or one – way ANOVA (non-parametric, Kruskal-Wallis test) followed by Dunns analysis or non-parametric t-test (Mann-Whitney's). Data are presented as mean ± SEM.

Table. 1

Age and diagnosis of the patients used in this study

Patients	Age	ESHF Diagnosis	CHD Diagnosis
1	3 mo	Congenital Cardiomyopathy (HLHS)	VSD
2	5 mo	Congenital Cardiomyopathy (DORV, UAVC)	VSD
3	8 mo	Congenital Cardiomyopathy (HLHS)	VSD
4	12.5mo	Dilated Cardiomyopathy (DCM)	VSD
5	1 year	Congenital Cardiomyopathy (HLHS)	VSD
6	13 mo	Dilated Cardiomyopathy	VSD
7	2 years	Dilated Cardiomyopathy	VSD
8	9 years	Dilated Cardiomyopathy	DNR
9	10 years	Dilated Cardiomyopathy	DNR
10	11years	Dilated Cardiomyopathy	DNR
11	12 years	Idiopathic Cardiomyopathy	DNR
12	12 years	Dilated Cardiomyopathy	DNR
13	13 years	Dilated Cardiomyopathy	DNR
14	14 years	Dilated Cardiomyopathy	DNR

ESHF = end-stage heart failure; **CHD** = control heart disease, **CCM** = congenital Burnt out cardiomyopathy; **DCM**=dilated cardiomyopathy; **ICM** = ischemic cardiomyopathy; **DNR** = Donor heart; **HLHS** = hypoplastic left heart syndrome; **DORV** = double outlet right ventricle; **UAVC** = unbalanced atrioventricular canal, **VSD** = ventricular septal defect